Fabrications of twisted moiré photonic crystal and random moiré photonic crystal and their potential applications in light extraction

Khadijah Alnasser,[1] Shan Li,[2] Siraj Sidhik,[3] Steve Kamau,[1] Jin Hou,[3] Noah Hurley,[1] Ayman Alzaid,[4] Sicheng Wang,[2] Hao Yan,[2] Jiangdong Deng,[5] Mohammad Omary,[2] Aditya D Mohite,[6,7] Jingbiao Cui,[1] and Yuankun Lin [1,8,*]

[1]*Department of Physics, University of North Texas, Denton, TX, USA*
[2]*Department of Chemistry, University of North Texas, Denton, TX, USA*
[3]*Department of Materials Science and NanoEngineering, Rice University, Houston, TX, USA*
[4]*Department of Computer Science, New Mexico State University, Las Cruces, NM 88003*
[5]*Center for Nanoscale Systems, Harvard University, Cambridge, MA 02138, USA*
[6]*Department of Chemical and Biomolecular Engineering, Rice University, Houston, TX, USA.*
[7]*Applied Physics Program, Smalley-Curl Institute, Rice University, Houston, TX, USA*
[8]*Department of Electrical Engineering, University of North Texas, Denton, TX, USA*
correspondence: yuankun.lin@unt.edu

Twisted moiré photonic crystal is an optical analog of twisted graphene or twisted transition metal dichalcogenide bilayers. In this paper, we report the fabrication of twisted moiré photonic crystals and randomized moiré photonic crystals and their use in enhanced extraction of light in LEDs. Fractional diffraction orders from randomized moiré photonic crystals are more uniform than those from moiré photonic crystals. Extraction efficiencies of 76.5%, 77.8% and 79.5% into glass substrate are predicted in simulations of LED patterned with twisted moiré photonic crystals, defect-containing photonic crystals and random moiré photonic crystals, respectively, at 584 nm. Extraction efficiencies of optically pumped LEDs with 2D perovskite $(BA)_2(MA)_{n-1}Pb_nI_{3n+1}$ of n=3 and (5-(2'-pyridyl)-tetrazolato)(3-CF_3-5-(2'-pyridyl)pyrazolato) platinum(II) (PtD) have been measured.

Keywords: E-beam lithography, twisted moiré photonic crystal, random moiré photonic crystal, light extraction efficiency,

Introduction

A photonic crystal (PhC) is a periodic nano/micro-structure where the refractive index is modulated periodically at the operating wavelength of light.[1] PhCs have been used to manipulate the light as a cavity, reflector, filter or a platform for photonics integration.[2–4] One example is the optical fiber grating (1D PhC) for a reflector and optical amplifier.[5,6] In 3D PhCs, a complete photonic bandgap can be achieved if all stop-bands form at the same frequency for all wavevectors.[7,8] Graded PhCs have been studied for light bending, nano-focus the light beam or cloaking device by arranging gradient filling fraction of dielectric materials in PhCs.[9–11] Recently, graded photonic super-crystals (GPSCs) have been produced through the eight-beam interference from two sets of four-beams arranged in different cone angles.[12] The GPSC has a gradient pattern, dual period, dual lattice and super-cell, leading toward a broadband optical response and large incident angle range for light coupling.[12–16] Very recently, it has been verified that GPSC is

actually a single-layer twisted moiré PhC.[17,18] The size (S) of the super-cell in GPSC (or twisted moiré PhC) is related to the twist angle α by $S=\Lambda/\tan(\alpha/2)$,[17,18] where Λ is the period of the traditional PhC. Twisted moiré PhC is an optical analog of twisted graphene or twisted transition metal dichalcogenide bilayers where significant interest has been triggered by the discovery of resonant modes, topological states, and flat photonic bands in moiré PhCs. [19–30]

Light-emitting diodes (LEDs) are 4th generation light sources with high efficiencies and long lifetimes.[31] For the organic LED, the internal quantum efficiency approaches almost 100% in small-molecule, phosphorescent materials. [32–35] However more than 50% of the generated light is wasted as a waveguide mode in the device or even worse as a surface plasmon mode at the cathode surface that becomes a hear source for the device. The light extraction layer is needed to improve the overall efficiency in LED. An extraction efficiency of 75% is targeted by the year 2035 by US Department of Energy. A gradient index layer on LED has reduced the total light reflection.[36–38] An incorporation of scatters such as meshed or nanoparticles was applied in LED.[39–42] Micro-lens arrays have been used to extract the waveguide mode in LED.[43–46] In order to reduce the loss in surface plasmon mode, light extractions through diffraction, scattering or coupling of surface plasmon polaritons (SPPs) into air mode have been effective using corrugated substrate or blazed gratings.[47–53] PhCs including GPSC as a group have shown promising for extracting light from both waveguide and SPP modes.[40,54–60] The simulation has predicted an extraction efficiency of 72% if the cathode of OLED is patterned with square GPSC and the extraction efficiency increases with the percentage of graded region over whole GPSC.[59] When the disorder is incorporated into the GPSC and metasurface, the broadband optical response, wide-angle coupling and high order Fourier frequency components can appear and be used for light extraction applications. [61–65]

In this paper we report the fabrication of twisted moiré PhCs and random moiré PhCs, and the simulated extraction efficiency of light into glass substrate from LED patterned with a twisted moiré PhC. By adding defects into the uniform area in the super-cell of moiré PhCs, the extraction efficiency can be improved. We further randomize the lattice positions in moiré PhC, and obtain more uniform diffraction pattern and higher extraction efficiency than these in regular moiré PhCs.

Experiments and simulations

Fabrication of PhCs: The twisted moiré PhC was fabricated by E-beam lithography (EBL). The design parameters for the hole size and location in the lattice were obtained from the eight-beam interference pattern that was generated by Matlab program. The unit super-cell is shown in **Figure S1a**. Iso-intensity surface was used for the determination of the hole size. The diameters for holes in rows #1 and #2 are also shown as examples. These design parameters were input into an E-beam exposure control program. A thickness of around 66 nm of polymethylmethacrylate (PMMA) was spin-coated on a Si substrate for 45 seconds with a speed of 3500 RPM using Laurell WS-650 tabletop spin coater. The sample was then post-baked at 180 ºC for 90 seconds. The thickness of 66 nm was estimated from a graph of the thickness versus the spin coating speed in the nanofabrication clean-room. The thickness of films in the graph was measured after the post-baking process. EBL pattern generator was used for EBL in JEOL JSM-7001F SEM machine. The sample was developed in a diluted solution of isopropanol and distilled water (3:1) for 10 seconds. The refractive index of PMMA might change after EBL.[66] The average refractive

index is 1.49 for PMMA in the visible range. For the randomized moiré PhC, we modified the design parameters for the position of holes in the twisted moiré PhC through a random number generator. For example, we changed x-component in the position (x, y) from 1000 nm to 985, 974, or 1050 nm; changed 2000 nm to 1978, 1956 or 2060 nm. In the simulation code, the random parameters were assigned to the position of holes in one quadrant of unit super-cell of random moire PhCs and these parameters were repeated for other three quadrants through an operation of mirror symmetry with x-axis or y-axis. One example of simulation code for assigned parameters in one quadrant is included in SI computation code-I for others to reproduce our results. The design of random moiré PhC is shown in **Figure S1b** where the positions are listed for holes in row #1 and #2 as examples.

Deposition of films and PL measurement: Deposition of (5-(2'-pyridyl)-tetrazolato)(3-CF_3-5-(2'-pyridyl)pyrazolato) platinum(II) (PtD) film[67] was performed inside Trovato 300C OLED fabrication system. A film of 2D Ruddlesden-Popper perovskites $(MA)_{n-1}Pb_nI_{3n+1}$ of n=3 where BA and MA standing for butylammonium and methylammonium, respectively) with a thickness of 300 nm was prepared as described in elsewhere.[68] The film is most optimized in terms of film quality and morphology (coverage).[68-69] $(MA)_{n-1}Pb_nI_{3n+1}$ of n=3 instead of n=1 or 2 was selected because its orientation[70] and PL from layer edge states[70-71] around 700 nm have been studied. The same thickness of 300 nm was also used for PtD film in this study. PLs from PtD with random moiré PhCs and without PhCs were measured with a Renishaw inVia Raman Microscope with a grating with a line densities of 1200 lines/mm, 473 nm laser and 50×/NA-0.50 microscope lens. PLs from 2D $(BA)_2(MA)_2Pb_3I_{10}$ film with and without moiré PhCs were measured with a different Renishaw inVia Raman Microscope with a grating with a line densities of 1800 lines/mm, 532 nm laser and 100×/NA-0.85 microscope lens. To make sure an almost same thickness for a valid comparison, the measurement locations for PL with and without PhCs are very close and in a same horizontal level as shown in **Fig. S2**. Ten PL sets of (without, edge, center and corner) were measured with a total number of 40 measurements for 2D perovskite $(BA)_2(MA)_2Pb_3I_{10}$ film. For PtD films, twelve PL sets of (with and without random moiré PhCs) were measured.

Results

Figure 1a shows the SEM of a fabricated twisted moiré PhC in PMMA with a 12Λ×12Λ super-cell as indicated by a red square, corresponding to a twist angle of 9.5 degrees, where Λ is labelled in the figure (Λ=1 μm). The edge, corner and center of the super-cell are labelled for the position of photoluminescence measurement. **Fig. 1b** shows the SEM of random moiré PhC in PMMA where the circle positions are randomly shifted from the regular moiré PhC. The dashed line indicates the position of one column of circles. For example, the circle positions indicated by blue and red arrows, however, are shifted toward left and right, respectively. A diffraction pattern of 532 nm laser from the twisted moiré PhC and random moiré PhC are shown in **Fig. 1c** and **1d,** respectively, where diffraction orders of (-1,-1) and (-2,0) are labelled. There is no diffraction maximum in first order diffractions of (±1,0) and (0,±1) as explained further in **Fig. 2**. Comparing diffractions in both figures, there is a strong secondary maximum around the diffraction maximum in **Fig. 1c** while the secondary maximum is not obviously visible in **Fig. 1d**. The diffraction pattern is more uniformly distributed in the fractional diffraction in **Fig. 1d** than that in **Fig. 1c**. We can see some weak fractional diffraction spots between the labels of (-2,2) and (0,2) in **Fig. 1c**. These

diffractions in both **Fig. 1c** and **Fig. 1d** can help decouple the light with p-polarization into the air mode through equation (1):[59]

$$k - m\frac{2\pi}{P} = \frac{2\pi}{\lambda}\sin\theta, \quad (1)$$

Where k is the wavevector of light, m the integral number, P the one of periods in moiré PhCs, λ wavelength of light, and θ the diffraction angle.

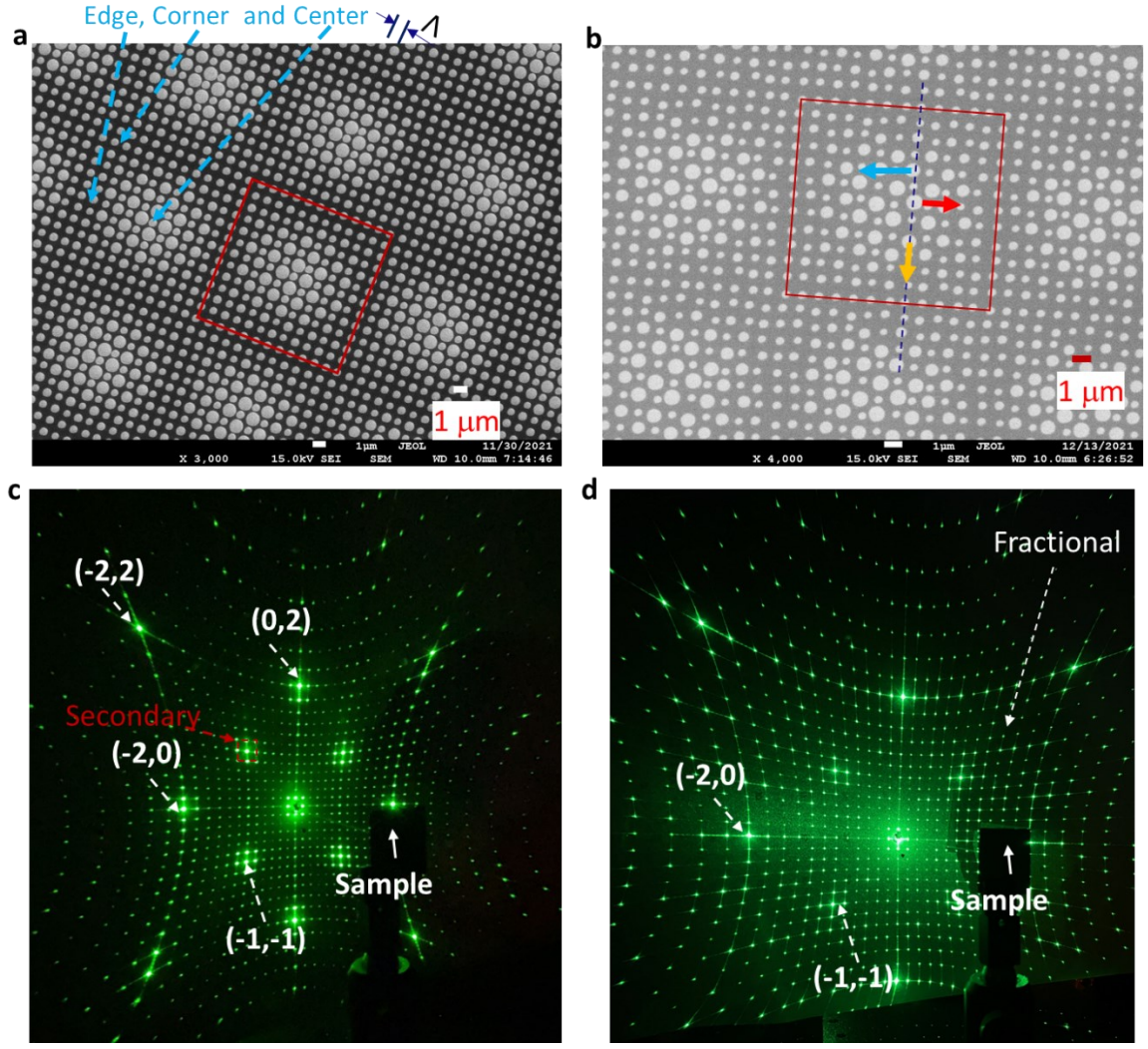

Fig. 1. (a) Scanning electron microscope (SEM) of fabricated twisted moiré PhC in PMMA with a thickness of 66 nm. The unit super-cell is indicated by a solid red square. Λ=1 μm. The positions for center, edge and corner of a super-cell are indicated. (b) SEM of fabricated random moiré PhC in PMMA. The unit super-cell is indicad by a solid red square. The position of circle is shifted toward left, right and up indicated by blue, red and yellow arrows, respectively. (c-d) 532 nm laser diffraction patterns for twisted moiré PhC (c) and random moiré PhC (d). Some 1st order and 2nd order diffraction spots and fractional diffraction are labelled.

For the LED with moiré PhC, an Al film is first deposited on top of the twisted moiré PhC and random moiré PhC. If we deposit light emitting material in the next step, the air cylinders in PhCs will take extra materials for light emitting. In order to have a reasonable comparison of PL intensity from the regions with and without PhC, we spin-coat 50 nm PMMA on the sample as shown in **Fig. S3** and then prepare 300 nm light emitter of PtD or 2D $(BA)_2(MA)_2Pb_3I_{10}$. Thus the structure has PMMA cylinders in Al background as shown in Fig. S3a. Al was selected in the study as it has been used in commercial products due to its low cost. In future, mask nano-patterning can print holes into organic layers and deposit Al into holes, thus forming Al cylinders in organic background. We simulate both cases of Al cylinders in organic background and organic cylinders in Al background and compare their results. The simulation of light in waveguide mode, SPP mode and glass substrate is performed using MIT MEEP,[72] a FDTD program run on Amazon Web Service's cloud computing platform. The structural parameters of the LED device in the simulation are listed in **Fig. S4a** where a glass substrate is added for the comparison of extraction efficiency in the traditional device and other simulations.[59] We set the refractive index of glass and light emitter to be 1.45 and 1.75, respectively. A calculated permittivity for $(BA)_2(MA)_2Pb_3I_{10}$ (one of light emitters) was used in the discussion section. The Drude-Lorentzian parameters for Al were obtained from a reference.[73] Simulation results for a glass thickness=10 μm and light emitter thickness=300 nm were almost same as those with thickness=1 μm and 200 nm, respectively.[60] All simulations in this study used structural parameters in Fig. S4a. The fractions of light in glass for dipole orientation perpendicular (E_z) to and parallel (E_x) to the LED layers are shown in **Fig. S4b** and **S4c**, respectively. As seen from the figures, the LED integrated with a PhC of organic (organic means PMMA thereafter) cylinders in Al background has a relatively higher efficiency than that with Al cylinders in organic background for wavelengths above 540 nm. Overall extraction efficiency of light into glass substrate is shown in **Fig. S4d**. There is no big difference in extraction efficiency whether the LED is integrated with organic cylinders or with Al cylinders. Their extraction efficiency can reach 76.5% at 584 nm.

The twisted moiré PhC has a gradient pattern in the center of super-cell for the destructive interference of SPP thus improving the extraction of light with s-polarization through equation (2):[59]

$$\mathrm{PL}\ \frac{2\pi}{\lambda}\ n_{eff} = m\,\pi + \beta, \qquad (2)$$

Where PL is the surface plasmon path length, n_{eff} the effective refractive index at dielectric/metal interface, λ the wavelength, m the integer number, and β the phase shift due to the reflection. Due to the gradient size of cylinders (or hole) and the destructive interference in Eq. (2), the SPP is localized within cylinders (holes) (as shown in Fig. 2a) with a similar size (as shown in Fig. 2b for a comparison of size and location of cylinders) for a certain wavelength. Furthermore, the simulation in Fig. 2a shows resonance directions in [1,1] and [0,2], however, does not support the resonance direction in [1,0], corresponding to strong diffraction spots at (1,1) and (0,2) and missing diffraction spots at (1,0) in Fig. 1c-d. As shown in Fig. 2c, the SPP loss over the total power in OLED varies with the twist angle (unit super-cell size) of moire PhCs. SPP loss is smaller at the twist angle of 9.5 degrees (unit super-cell size $12\Lambda \times 12\Lambda$) than other angles. We focus on the moire PhCs with a unit super-cell size $12\Lambda \times 12\Lambda$ in this study.

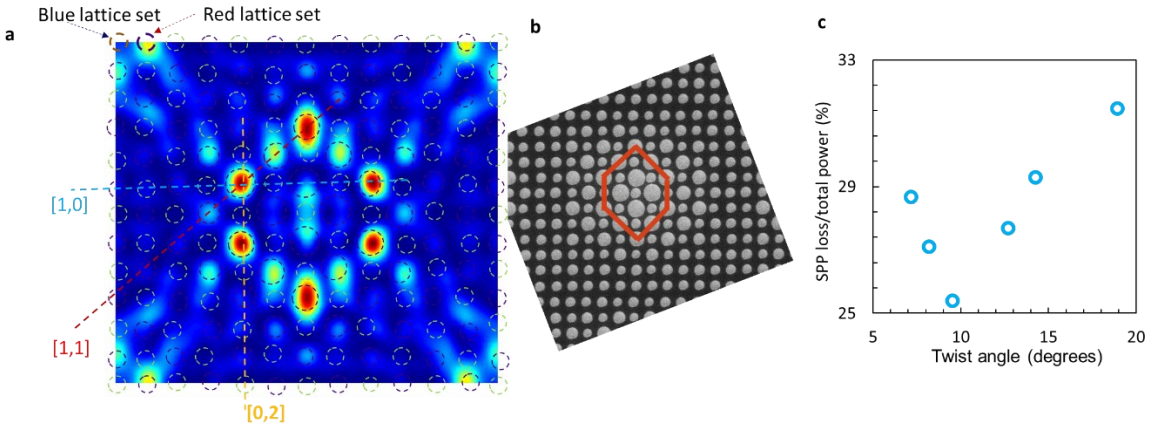

Fig. 2: (a) Simulated electric field intensity in the organic materials above the metallic layer. (b) A schematic showing the SPP resonance path for a comparison with the SPP pattern in (a). (c) Calculated SPP loss over the total power in OLED integrated with moire PhCs with different twist angles.

This idea in equation (2) is further tested by destroying the relatively uniform pattern at the edge and corner of the super-cell through placing 4 defects, each at the edge and corner as shown in insets for Al cylinders and organic cylinders-type PhCs in **Fig. 3a** and **3b**, respectively. The addition of these defects changes the uniform regions into a non-uniform region for a destructive SPP resonance. When comparing the fraction of light in glass with defects in twisted moiré PhC and that without defects (regular twisted moiré PhC), there is no big change for dipoles with E_z polarization. For dipoles with E_x polarization, the fraction of light in glass is higher in PhCs with defects than those without defects in longer wavelengths above 500 nm in **Fig. 3a.** The overall extraction efficiency of light into glass is 77.7% at 584 nm in **Fig. 3b**.

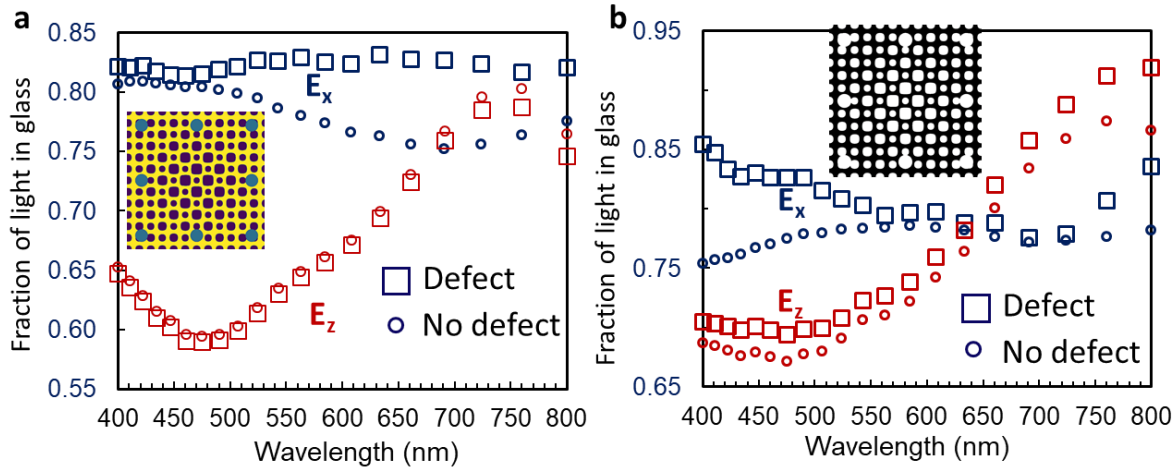

Fig. 3. Simulated fraction of light in glass substrate for dipole orientations perpendicular to (red symbols)) and parallel to (blue symbols) the layers of LED with PhCs of Al cylinders in organic background (a) and organic cylinders in Al background (b) that contain defects at 8 locations (squares), compared with these

without defects (circles). Insets are the moiré PhCs with defects at 8 locations for the purpose of generating less uniform pattern.

We now compare the simulation prediction with experimental results. **Fig. 4a** shows the PL measurement from 2D perovskite $(BA)_2(MA)_2Pb_3I_{10}$ film in LED layers integrated with twisted moiré PhCs and without PhCs, and their intensity ratio (solid red line, in secondary y-axis). The empty squares correspond to the simulated intensity ratio assuming that 93.4% of the dipole orientations are in horizontal direction parallel to the LED layer, as calculated from polarized PLs in a reference.[74] The 2D layered structure in $(BA)_2(MA)_2Pb_3I_{10}$ film is perpendicular to the substrate,[70] as shown in **Fig. S5a,** and therefore the PL is highly polarized.[67,74,75] The ratio of PL intensity from $(BA)_2(MA)_2Pb_3I_{10}$ film integrated with twisted moiré PhCs over that without moiré PhCs is measured to be between 1.3 and 1.9 in a wavelength range of 670-760 nm, comparing with the predicted ratios between 1.68 and 1.76. Near the PL maximum around 700 nm, the simulated PL intensity ratio is 1.68 versus 1.47 in measurement in **Fig. 4a**.

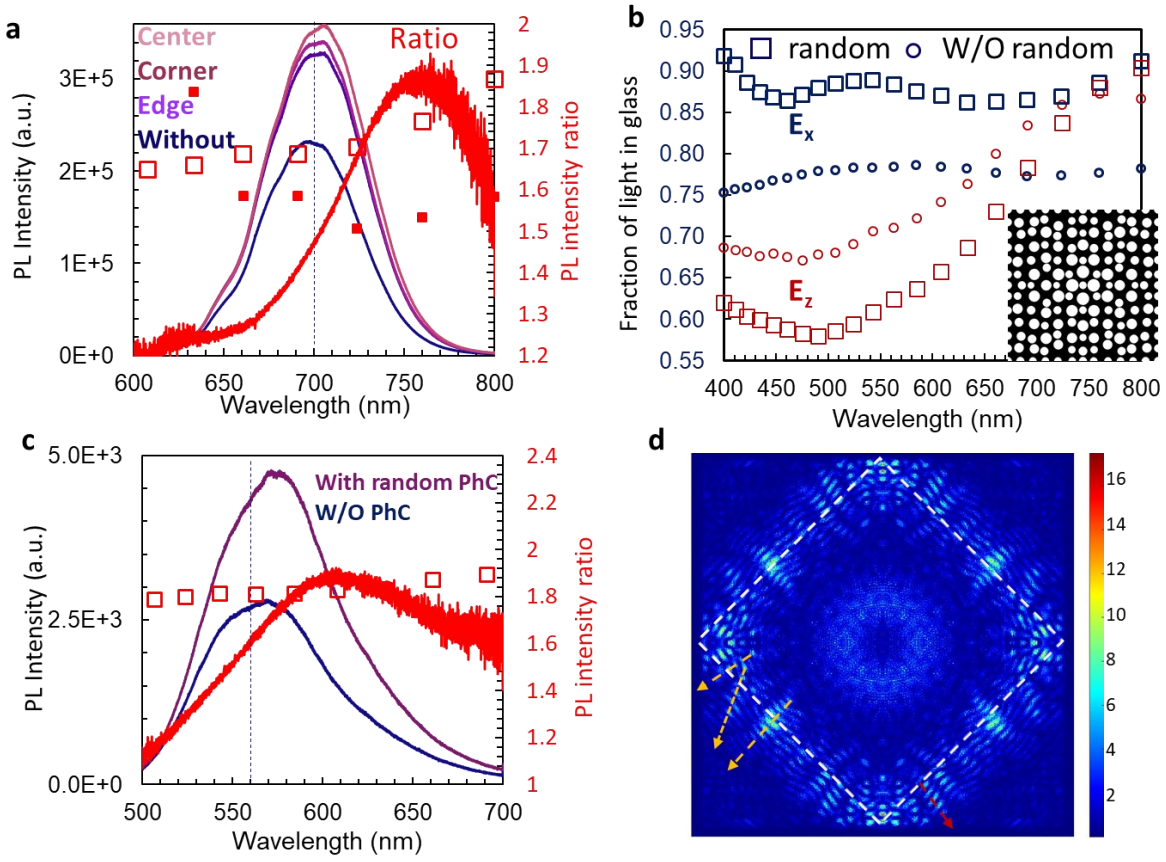

Fig. 4. (a) PLs from 2D $(BA)_2(MA)_2Pb_3I_{10}$ LED layers integrated twisted moiré PhC measured at the center, corner and edge of the unit super-cell, PL from LED layers without moiré PhC (blue line), and ratio of average PL intensity with moiré PhC over that without PhC, comparing with the simulated intensity ratio for 2D $(BA)_2(MA)_2Pb_3I_{10}$ with 93.4% E_x dipole with a constant refractive index (empty red squares) and a calculated permittivity in the discussion section (solid red squares). (b) Simulated fraction of light in glass substrate for dipole orientations perpendicular to (red symbols)) and parallel to (blue symbols) the layers

of LED for moiré PhCs with random position of organic cylinders in Al background (squares), compared with these in moiré PhC without random positions (circles). Inset is the simulation generated random moiré PhC. (c) Measured PLs from PtD LED layers integrated with random moiré PhC (orange line), without PhC (blue line) and their intensity ratio (red line), comparing with the simulated intensity ratio for PtD with 92% of dipoles in parallel to the LED layer (empty red squares). (d) Computed E-field intensity distribution in the glass substrate in LED integrated with random moiré PhCs.

We further randomized the lattice position in moiré PhCs. We simulated the light extraction into the glass substrate from the LED layers when the LED is patterned with random moiré PhCs. As shown in **Fig. 4b**, the fraction of light in glass for Ex dipole is higher in structures with random moiré PhCs than those without random lattice (i.e. regular moiré PhCs), while the fraction of light in glass is lower for Ez dipole in structures with random moiré PhCs than those with regular moiré PhCs. The overall extraction efficiency of light into glass substrate is 79.5% at 584 nm. PLs from PtD film in LED integrated with random moiré PhC and without PhC (blue line) are shown in **Fig. 4c** and their intensity ratio is plotted in a red line. The ordered arrangement of PtD film is schematically illustrated in Fig. S5a.[70,75] With 92% of dipoles in Ex polarization as measured by angle-dependent PL method,[76] the simulated intensity ratio is between 1.80 and 1.87, while the measured ratio is between 1.25 and 1.88 for the wavelength range of 520-670 nm in **Fig. 4c**. At the peak center near 571 nm, the measured PL intensity ratio is 1.69, in comparison with the simulated intensity ratio of versus 1.81.

We also computed the E-field intensity in the glass substrate in **Fig. 4d** during the simulation in **Fig. 4b** when the LED is integrated with random moiré PhCs. Although the lattice position is randomly shifted from the regular moiré PhCs, the square symmetry is retained as seen from the square shape indicated by the dashed white square in **Fig. 4d**. The light travels in different directions as indicated by the dash arrows in **Fig. 4d**, as expected, due to the randomized lattice.

Discussions

Firstly, we discuss the effect of randomization. In this study, the lattice position is randomized by less than 5% of the period (which is 1000 nm). Following the **Eq. (1),** the decoupling of light with E_z polarization into air mode is weakened due to the destruction of the periodicity of the lattices. It can explain why the extraction efficiency from LED integrated with random moiré PhCs is less than that with regular moiré PhCs for E_z polarization in **Fig. 4b**. The resonance condition in **Eq. (2)** for $E_{x,y}$ polarization is further destroyed in randomized lattices in random moiré PhCs. It can explain the higher extraction efficiency from LED integrated with random moiré PhCs than that with regular moiré PhCs in **Fig. 4b**. Although the extraction efficiency drops for E_z polarization, the overall extraction efficiency is higher in LED with random moiré PhC than that with regular moiré PhC, as shown in **Fig. S6**. For example, the extraction efficiency is 79.6% at a wavelength of 584 nm for random moiré PhC case compared to 76.5% for regular moiré PhC case. The predicted increase of extraction efficiency from regular moiré PhC, to defect-containing moiré PhC, and to random moiré PhC, is due to the increased number of

photonic modes in these PhCs.[77] Experimentally, we observed an intensity increase of 1.47 and 1.69 in LED with regular moiré PhC and random moiré PhC, comparing with that without PhCs.

Next, we discuss the disagreement between simulation and experimental results. The simulation shows an almost equivalent PL intensity ratio in the measured PL range, while the experimental data show an increasing intensity ratio from short to long PL wavelengths, with a maximum ratio in the long wavelength side, as shown in **Fig. 4a** and **4c**. We used a constant refractive index of 1.75 for the simulation in **Fig. 4a** and **4c**. In order to have an accurate simulation, the permittivity of PtD and 2D perovskite and their dispersion need to be included in the simulation. Our co-authors have published the refractive index n and k for 2D Ruddlesden-Popper perovskites $(MA)_{n-1}Pb_nI_{3n+1}$ of n=3 using a combined Tauc-Lorentz model.[78] We used Drude-Lorentz model[79] in Eq. (3) to fit their data using one Lorentz term:

$$\varepsilon(\omega) = \varepsilon_b - \frac{\omega_p^2}{\omega^2 + i\Gamma_p\omega} + \frac{f_1\omega_1^2}{\omega_1^2 - \omega^2 - i\Gamma_1\omega} \qquad (3)$$

We applied the published parameters:[78] $\varepsilon_b = 5.3$ for the background permittivity, $\Gamma_p = 0.06\ eV$ for the carrier relaxation rate, and $f_1 = 0.35$ for the strength of the Lorentz oscillator. We selected center frequency $\omega_1 = 1.77\ eV$ for the PL central frequency, relaxation $\Gamma_1 = 0.17\ eV$ for the Lorentz oscillation line width, and the unscreened plasma frequency $\omega_p = 1.3\ eV$ for the real permittivity close to 5 around 900 nm. The generated permittivity is shown in Fig. 5 that can catch necessary features near 700 nm. The simulated light intensity ratio is 1.58 (1.5) at 690 (723) nm, very close to the measured PL ratio at the central wavelength. The simulated ratio in a large range is included in Fig. 4a.

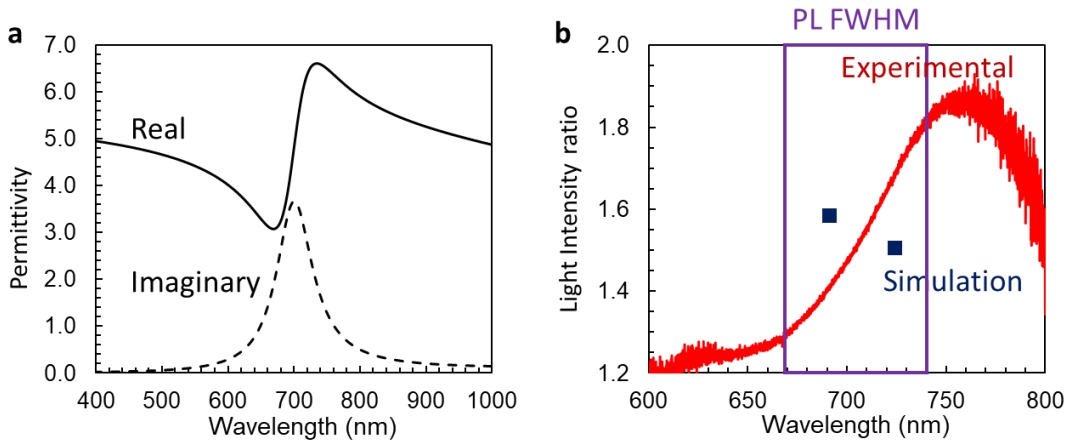

Fig. 5. (a) Calculated dielectric function spectra for 2D $(BA)_2(MA)_2Pb_3I_{10}$ using Drude-Lorentz model. (b) The ratio of PL from $(BA)_2(MA)_2Pb_3I_{10}$ integrated with moiré PhC over that without PhC, comparing with the simulated intensity ratio (solid blue squares) in the PL range of full width half maximum.

We further discuss the Ex and Ez polarization effects. The waveguide mode can be easily reduced by integrating patterns in the LED. The coupling of E_z polarized light into air mode can be enhanced through multiple periodicities in moiré PhCs. The destructive interference of SPP can

increase the extraction efficiency for light with $E_{x,y}$ polarizations. PL from PtD or 2D perovskites are highly Ex,y polarized. It is nice to use these materials to test the theory governed by **Eq (1)** and **(2)** individually. However, the simulation needs a full verification by using other materials although it predicts an extraction efficiency above the targeted 75% as set for year 2035 by Department of Energy. In future, nonlinear optical properties in moire photonic crystals can also be included to advance the research in this field.[80]

Conclusion

We have fabricated twisted moiré photonic crystals and randomized moiré photonic crystals through e-beam lithography, and simulated light extraction efficiencies of 76.5%, 77.8% and 79.5% into the glass substrate for an LED integrated with a twisted moiré PhC, defect-containing moiré PhC and random moiré PhC, respectively. We have measured and obtained ratios of light intensity of LED integrated with a twisted moiré photonic crystal and a random moiré photonic crystal over that without moiré photonic crystal, that are 1.47 (perovskite) and 1.69 (PtD), respectively, comparing with the predicted ratios of 1.68 and 1.81 at the central PL wavelength. The material dispersion needs to be further included for an accurate prediction.

Conflict of Interest

The authors declare no competing financial interest. This report was prepared as an account of work sponsored by an agency of the United States Government. Neither the United States Government nor any agency thereof, nor any of their employees, makes any warranty, express or implied, or assumes any legal liability or responsibility for the accuracy, completeness, or usefulness of any information, apparatus, product, or process disclosed, or represents that its use would not infringe privately owned rights. Reference herein to any specific commercial product, process, or service by trade name, trademark, manufacturer, or otherwise does not necessarily constitute or imply its endorsement, recommendation, or favoring by the United States Government or any agency thereof. The views and opinions of authors expressed herein do not necessarily state or reflect those of the United States Government or any agency thereof.

Acknowledgments

This work was supported by the U.S. National Science Foundation (#2128367). This work was performed in part at the University of North Texas's Materials Research Facility: A shared research facility for multi-dimensional fabrication and characterization and with the assistance of Dr. Jianchao Li.

Supporting Information

Descriptions of designs of moiré photonic crystal and random moiré photonic crystal, methods of multiple measurements, details on LED structures with and without photonic crystal, calculations of light extraction efficiency of the LED with moiré photonic crystal, sample orientations on the substrate, calculations of light extraction efficiency of the LED with random moiré photonic crystal.

References

(1) John, S. Strong Localization of Photons in Certain Disordered Dielectric Superlattices. *Phys Rev Lett* **1987**, *58* (23). https://doi.org/10.1103/PhysRevLett.58.2486.

(2) Kuramochi, E.; Nozaki, K.; Shinya, A.; Takeda, K.; Sato, T.; Matsuo, S.; Taniyama, H.; Sumikura, H.; Notomi, M. Large-Scale Integration of Wavelength-Addressable All-Optical Memories on a Photonic Crystal Chip. *Nat Photonics* **2014**, *8* (6). https://doi.org/10.1038/nphoton.2014.93.

(3) Li, M.; Ling, J.; He, Y.; Javid, U. A.; Xue, S.; Lin, Q. Lithium Niobate Photonic-Crystal Electro-Optic Modulator. *Nat Commun* **2020**, *11* (1). https://doi.org/10.1038/s41467-020-17950-7.

(4) Lončar, M.; Yoshie, T.; Scherer, A.; Gogna, P.; Qiu, Y. Low-Threshold Photonic Crystal Laser. *Appl Phys Lett* **2002**, *81* (15). https://doi.org/10.1063/1.1511538.

(5) Chartier, T. Optical Fibers. In *Springer Handbooks*; 2019. https://doi.org/10.1007/978-3-319-93728-1_41.

(6) Tian, X.; Zhao, X.; Wang, M.; Wang, Z. Suppression of Stimulated Brillouin Scattering in Optical Fibers by Tilted Fiber Bragg Gratings. *Opt Lett* **2020**, *45* (17). https://doi.org/10.1364/ol.401433.

(7) Ishizaki, K.; Noda, S. Manipulation of Photons at the Surface of Three-Dimensional Photonic Crystals. *Nature* **2009**, *460* (7253). https://doi.org/10.1038/nature08190.

(8) Fleming, J. G.; Lin, S. Y.; El-Kady, I.; Biswas, R.; Ho, K. M. All-Metallic Three-Dimensional Photonic Crytal with a Large Infrared Bandgap. *Nature* **2002**, *417* (6884). https://doi.org/10.1038/417052a.

(9) Ergin, T.; Stenger, N.; Brenner, P.; Pendry, J. B.; Wegener, M. Three-Dimensional Invisibility Cloak at Optical Wavelengths. *Science (1979)* **2010**, *328*, 337339. https://doi.org/10.1126/science.1186351.

(10) Li, Y. H.; Fu, Y. Q.; Minin, O. v.; Minin, I. v. Ultra-Sharp Nanofocusing of Graded Index Photonic Crystal-Based Lenses Perforated with Optimized Single Defect. *Opt Mater Express* **2016**, *6* (8). https://doi.org/10.1364/ome.6.002628.

(11) Vasic, B.; Isic, G.; Gajic, R.; Hingerl, K. Controlling Electromagnetic Fields with Graded Photonic Crystals in Metamaterial Regime. *Opt Express* **2010**, *18* (19). https://doi.org/10.1364/oe.18.020321.

(12) Lowell, D.; Lutkenhaus, J.; George, D.; Philipose, U.; Chen, B.; Lin, Y. Simultaneous Direct Holographic Fabrication of Photonic Cavity and Graded Photonic Lattice with Dual Periodicity, Dual Basis, and Dual Symmetry. *Opt Express* **2017**, *25* (13). https://doi.org/10.1364/oe.25.014444.

(13) Hassan, S.; Alnasser, K.; Lowell, D.; Lin, Y. Effects of Photonic Band Structure and Unit Super-Cell Size in Graded Photonic Super-Crystal on Broadband Light Absorption in Silicon. *Photonics* **2019**, *6* (2). https://doi.org/10.3390/photonics6020050.

(14) Lowell, D.; Hassan, S.; Adewole, M.; Philipose, U.; Chen, B.; Lin, Y. Holographic Fabrication of Graded Photonic Super-Crystals Using an Integrated Spatial Light Modulator and Reflective Optical Element Laser Projection System. *Appl Opt* **2017**, *56* (36). https://doi.org/10.1364/ao.56.009888.

(15) Hassan, S.; Sale, O.; Alnasser, K.; Hurley, N.; Zhang, H.; Philipose, U.; Lin, Y. Broadband Light-Matter Interaction Due to Resonance Cavities in Graded Photonic Super-Crystals. *OSA Contin* **2019**, *2* (11). https://doi.org/10.1364/osac.2.003272.

(16) Hassan, S.; Jiang, Y.; Alnasser, K.; Hurley, N.; Zhang, H.; Philipose, U.; Lin, Y. Generation of over 1000 Diffraction Spots from 2D Graded Photonic Super-Crystals. *Photonics* **2020**, *7* (2). https://doi.org/10.3390/PHOTONICS7020027.

(17) Alnasser, K.; Kamau, S.; Hurley, N.; Cui, J.; Lin, Y. Photonic Band Gaps and Resonance Modes in 2d Twisted Moiré Photonic Crystal. *Photonics* **2021**, *8* (10). https://doi.org/10.3390/photonics8100408.

(18) Alnasser, K.; Kamau, S.; Hurley, N.; Cui, J.; Lin, Y. Resonance Modes in Moiré Photonic Patterns for Twistoptics. *OSA Contin* **2021**, *4* (4). https://doi.org/10.1364/osac.420912.

(19) Lou, B.; Zhao, N.; Minkov, M.; Guo, C.; Orenstein, M.; Fan, S. Theory for Twisted Bilayer Photonic Crystal Slabs. *Phys Rev Lett* **2021**, *126* (13). https://doi.org/10.1103/PhysRevLett.126.136101.

(20) Tang, H.; Du, F.; Carr, S.; DeVault, C.; Mello, O.; Mazur, E. Modeling the Optical Properties of Twisted Bilayer Photonic Crystals. *Light Sci Appl* **2021**, *10* (1). https://doi.org/10.1038/s41377-021-00601-x.

(21) Lou, B.; Fan, S. Tunable Frequency Filter Based on Twisted Bilayer Photonic Crystal Slabs. *ACS Photonics* **2022**, *9* (3). https://doi.org/10.1021/acsphotonics.1c01263.

(22) Dong, K.; Zhang, T.; Li, J.; Wang, Q.; Yang, F.; Rho, Y.; Wang, D.; Grigoropoulos, C. P.; Wu, J.; Yao, J. Flat Bands in Magic-Angle Bilayer Photonic Crystals at Small Twists. *Phys Rev Lett* **2021**, *126* (22). https://doi.org/10.1103/PhysRevLett.126.223601.

(23) Sánchez-Ochoa, F.; Hidalgo, F.; Pruneda, M.; Noguez, C. Unfolding Method for Periodic Twisted Systems with Commensurate Moiré Patterns. *Journal of Physics Condensed Matter* **2020**, *32* (2). https://doi.org/10.1088/1361-648X/ab44f0.

(24) Gómez-Urrea, H. A.; Ospina-Medina, M. C.; Correa-Abad, J. D.; Mora-Ramos, M. E.; Caro-Lopera, F. J. Tunable Band Structure in 2D Bravais–Moiré Photonic Crystal Lattices. *Opt Commun* **2020**, *459*. https://doi.org/10.1016/j.optcom.2019.125081.

(25) Wang, P.; Zheng, Y.; Chen, X.; Huang, C.; Kartashov, Y. v.; Torner, L.; Konotop, V. v.; Ye, F. Localization and Delocalization of Light in Photonic Moiré Lattices. *Nature* **2020**, *577* (7788). https://doi.org/10.1038/s41586-019-1851-6.

(26) Chen, J.; Lin, X.; Chen, M.; Low, T.; Chen, H.; Dai, S. A Perspective of Twisted Photonic Structures. *Appl Phys Lett* **2021**, *119* (24). https://doi.org/10.1063/5.0070163.

(27) Ebnonnasir, A.; Narayanan, B.; Kodambaka, S.; Ciobanu, C. v. Tunable MoS2 Bandgap in MoS2-Graphene Heterostructures. *Appl Phys Lett* **2014**, *105* (3). https://doi.org/10.1063/1.4891430.

(28) Zeng, J.; Hu, Y.; Zhang, X.; Fu, S.; Yin, H.; Li, Z.; Chen, Z. Localization-to-Delocalization Transition of Light in Frequency-Tuned Photonic Moiré Lattices. *Opt Express* **2021**, *29* (16). https://doi.org/10.1364/oe.434281.

(29) Fu, Q.; Wang, P.; Huang, C.; Kartashov, Y. v.; Torner, L.; Konotop, V. v.; Ye, F. Optical Soliton Formation Controlled by Angle Twisting in Photonic Moiré Lattices. *Nat Photonics* **2020**, *14* (11). https://doi.org/10.1038/s41566-020-0679-9.

(30) Chen, M. K.; Zhang, J. C.; Leung, C. W.; Sun, L.; Fan, Y.; Liang, Y.; Yao, J.; Liu, X.; Yuan, J.; Xu, Y.; Tsai, D. P.; Pang, S. W. Chiral-Magic Angle of Nanoimprint Meta-Device. *Nanophotonics* **2023**. https://doi.org/10.1515/nanoph-2022-0733.

(31) Pimputkar, S.; Speck, J. S.; Denbaars, S. P.; Nakamura, S. Prospects for LED Lighting. *Nature Photonics*. 2009. https://doi.org/10.1038/nphoton.2009.32.

(32) Bhansali, U. S.; Polikarpov, E.; Swensen, J. S.; Chen, W. H.; Jia, H.; Gaspar, D. J.; Gnade, B. E.; Padmaperuma, A. B.; Omary, M. A. High-Efficiency Turquoise-Blue Electrophosphorescence from a Pt(II)-Pyridyltriazolate Complex in a Phosphine Oxide Host. *Appl Phys Lett* **2009**, *95* (23). https://doi.org/10.1063/1.3268434.

(33) Adachi, C.; Baldo, M. A.; Thompson, M. E.; Forrest, S. R. Nearly 100% Internal Phosphorescence Efficiency in an Organic Light Emitting Device. *J Appl Phys* **2001**, *90* (10). https://doi.org/10.1063/1.1409582.

(34) Baldo, M. A.; O'Brien, D. F.; You, Y.; Shoustikov, A.; Sibley, S.; Thompson, M. E.; Forrest, S. R. Highly Efficient Phosphorescent Emission from Organic Electroluminescent Devices. *Nature* **1998**, *395* (6698). https://doi.org/10.1038/25954.

(35) Reineke, S.; Lindner, F.; Schwartz, G.; Seidler, N.; Walzer, K.; Lüssem, B.; Leo, K. White Organic Light-Emitting Diodes with Fluorescent Tube Efficiency. *Nature* **2009**, *459* (7244). https://doi.org/10.1038/nature08003.

(36) Ma, M.; Cho, J.; Schubert, E. F.; Kim, G. B.; Sone, C. Optically Functional Surface Structures for GaN-Based Light-Emitting Diodes. *J Mater Chem C Mater* **2013**, *1* (48). https://doi.org/10.1039/c3tc31620c.

(37) Sajeev, A. K.; Agarwal, N.; Soman, A.; Gupta, S.; Katiyar, M.; Ajayaghosh, A.; Unni, K. N. N. Enhanced Light Extraction from Organic Light Emitting Diodes Using a Flexible Polymer-Nanoparticle Scattering Layer. *Org Electron* **2022**, *100*. https://doi.org/10.1016/j.orgel.2021.106386.

(38) Salehi, A.; Chen, Y.; Fu, X.; Peng, C.; So, F. Manipulating Refractive Index in Organic Light-Emitting Diodes. *ACS Appl Mater Interfaces* **2018**, *10* (11). https://doi.org/10.1021/acsami.7b18514.

(39) Koh, T. W.; Spechler, J. A.; Lee, K. M.; Arnold, C. B.; Rand, B. P. Enhanced Outcoupling in Organic Light-Emitting Diodes via a High-Index Contrast Scattering Layer. *ACS Photonics* **2015**, *2* (9). https://doi.org/10.1021/acsphotonics.5b00346.

(40) Oskooi, A. Texturing the Cathode of White Organic Light-Emitting Diodes with a Lattice of Nanoscale Scatterers for Enhanced Light out-Coupling. *Appl Phys Lett* **2015**, *106* (4). https://doi.org/10.1063/1.4907253.

(41) Song, J.; Kim, K. H.; Kim, E.; Moon, C. K.; Kim, Y. H.; Kim, J. J.; Yoo, S. Lensfree OLEDs with over 50% External Quantum Efficiency via External Scattering and Horizontally Oriented Emitters. *Nat Commun* **2018**, *9* (1). https://doi.org/10.1038/s41467-018-05671-x.

(42) Cheng, Y. H.; Wu, J. L.; Cheng, C. H.; Syao, K. C.; Lee, M. C. M. Enhanced Light Outcoupling in a Thin Film by Texturing Meshed Surfaces. *Appl Phys Lett* **2007**, *90* (9). https://doi.org/10.1063/1.2709920.

(43) Qu, Y.; Kim, J.; Coburn, C.; Forrest, S. R. Efficient, Nonintrusive Outcoupling in Organic Light Emitting Devices Using Embedded Microlens Arrays. *ACS Photonics* **2018**, *5* (6). https://doi.org/10.1021/acsphotonics.8b00255.

(44) Han, K. H.; Park, Y. S.; Cho, D. H.; Han, Y.; Lee, J.; Yu, B.; Cho, N. S.; Lee, J. I.; Kim, J. J. Optical Analysis of Power Distribution in Top-Emitting Organic Light Emitting Diodes Integrated with Nanolens Array Using Finite Difference Time Domain. *ACS Appl Mater Interfaces* **2018**, *10* (22). https://doi.org/10.1021/acsami.8b02631.

(45) Park, W.-Y.; Kwon, Y.; Lee, C.; Whang, K.-W. Light Outcoupling Enhancement from Top-Emitting Organic Light-Emitting Diodes Made on a Nano-Sized Stochastic Texture Surface. *Opt Express* **2014**, *22* (S7). https://doi.org/10.1364/oe.22.0a1687.

(46) Zhou, L.; Ou, Q. D.; Chen, J. de; Shen, S.; Tang, J. X.; Li, Y. Q.; Lee, S. T. Light Manipulation for Organic Optoelectronics Using Bio-Inspired Moth's Eye Nanostructures. *Sci Rep* **2014**, *4*. https://doi.org/10.1038/srep04040.

(47) Will, P. A.; Schmidt, M.; Eckhardt, K.; Wisser, F.; Lenk, S.; Grothe, J.; Kaskel, S.; Reineke, S. Efficiency of Light Outcoupling Structures in Organic Light-Emitting Diodes: 2D TiO 2 Array as a Model System. *Adv Funct Mater* **2019**, *29* (20). https://doi.org/10.1002/adfm.201901748.

(48) Fu, X.; Mehta, Y.; Chen, Y. A.; Lei, L.; Zhu, L.; Barange, N.; Dong, Q.; Yin, S.; Mendes, J.; He, S.; Gogusetti, R.; Chang, C. H.; So, F. Directional Polarized Light Emission from Thin-Film Light-Emitting Diodes. *Advanced Materials* **2021**, *33* (9). https://doi.org/10.1002/adma.202006801.

(49) Lim, T.-B.; Cho, K. H.; Kim, Y.-H.; Jeong, Y.-C. Enhanced Light Extraction Efficiency of OLEDs with Quasiperiodic Diffraction Grating Layer. *Opt Express* **2016**, *24* (16). https://doi.org/10.1364/oe.24.017950.

(50) Liang, H.; Hsu, H.-C.; Wu, J.; He, X.; Wei, M.-K.; Chiu, T.-L.; Lin, C.-F.; Lee, J.-H.; Wang, J. Corrugated Organic Light-Emitting Diodes to Effectively Extract Internal Modes. *Opt Express* **2019**, *27* (8). https://doi.org/10.1364/oe.27.00a372.

(51) Koo, W. H.; Jeong, S. M.; Araoka, F.; Ishikawa, K.; Nishimura, S.; Toyooka, T.; Takezoe, H. Light Extraction from Organic Light-Emitting Diodes Enhanced by Spontaneously Formed Buckles. *Nat Photonics* **2010**, *4* (4). https://doi.org/10.1038/nphoton.2010.7.

(52) Youn, W.; Lee, J.; Xu, M.; Singh, R.; So, F. Corrugated Sapphire Substrates for Organic Light-Emitting Diode Light Extraction. *ACS Appl Mater Interfaces* **2015**, *7* (17). https://doi.org/10.1021/acsami.5b01533.

(53) Jiao, B.; Yu, Y.; Dai, Y.; Hou, X.; Wu, Z. Improvement of Light Extraction in Organic Light-Emitting Diodes Using a Corrugated Microcavity. *Opt Express* **2015**, *23* (4). https://doi.org/10.1364/oe.23.004055.

(54) McGroddy, K.; David, A.; Matioli, E.; Iza, M.; Nakamura, S.; Denbaars, S.; Speck, J. S.; Weisbuch, C.; Hu, E. L. Directional Emission Control and Increased Light Extraction in GaN Photonic Crystal Light Emitting Diodes. *Appl Phys Lett* **2008**, *93* (10). https://doi.org/10.1063/1.2978068.

(55) Matioli, E.; Rangel, E.; Iza, M.; Fleury, B.; Pfaff, N.; Speck, J.; Hu, E.; Weisbuch, C. High Extraction Efficiency Light-Emitting Diodes Based on Embedded Air-Gap Photonic-Crystals. *Appl Phys Lett* **2010**, *96* (3). https://doi.org/10.1063/1.3293442.

(56) Truong, T. A.; Campos, L. M.; Matioli, E.; Meinel, I.; Hawker, C. J.; Weisbuch, C.; Petroff, P. M. Light Extraction from GaN-Based Light Emitting Diode Structures with a Noninvasive Two-Dimensional Photonic Crystal. *Appl Phys Lett* **2009**, *94* (2). https://doi.org/10.1063/1.3067837.

(57) Boroditsky, M.; Krauss, T. F.; Coccioli, R.; Vrijen, R.; Bhat, R.; Yablonovitch, E. Light Extraction from Optically Pumped Light-Emitting Diode by Thin-Slab Photonic Crystals. *Appl Phys Lett* **1999**, *75* (8). https://doi.org/10.1063/1.124588.

(58) Wiesmann, C.; Bergenek, K.; Linder, N.; Schwarz, U. T. Photonic Crystal LEDs - Designing Light Extraction. *Laser and Photonics Reviews*. 2009. https://doi.org/10.1002/lpor.200810053.

(59) Alnasser, K.; Hassan, S.; Kamau, S.; Zhang, H.; Lin, Y. Enhanced Light Extraction from Organic Light-Emitting Diodes by Reducing Plasmonic Loss through Graded Photonic Super-Crystals. *Journal of the Optical Society of America B* **2020**, *37* (5). https://doi.org/10.1364/josab.387780.

(60) Hassan, S.; Lowell, D.; Lin, Y. High Light Extraction Efficiency into Glass Substrate in Organic Light-Emitting Diodes by Patterning the Cathode in Graded Superlattice with Dual Periodicity and Dual Basis. *J Appl Phys* **2017**, *121* (23). https://doi.org/10.1063/1.4986233.

(61) Vynck, K.; Burresi, M.; Riboli, F.; Wiersma, D. S. Photon Management in Two-Dimensional Disordered Media. *Nat Mater* **2012**, *11* (12). https://doi.org/10.1038/nmat3442.

(62) Mao, P.; Liu, C.; Li, X.; Liu, M.; Chen, Q.; Han, M.; Maier, S. A.; Sargent, E. H.; Zhang, S. Single-Step-Fabricated Disordered Metasurfaces for Enhanced Light Extraction from LEDs. *Light Sci Appl* **2021**, *10* (1). https://doi.org/10.1038/s41377-021-00621-7.

(63) Oskooi, A.; Favuzzi, P. A.; Tanaka, Y.; Shigeta, H.; Kawakami, Y.; Noda, S. Partially Disordered Photonic-Crystal Thin Films for Enhanced and Robust Photovoltaics. *Appl Phys Lett* **2012**, *100* (18). https://doi.org/10.1063/1.4711144.

(64) Oskooi, A.; Tanaka, Y.; Noda, S. Tandem Photonic-Crystal Thin Films Surpassing Lambertian Light-Trapping Limit over Broad Bandwidth and Angular Range. *Appl Phys Lett* **2014**, *104* (9). https://doi.org/10.1063/1.4867892.

(65) Jang, M.; Horie, Y.; Shibukawa, A.; Brake, J.; Liu, Y.; Kamali, S. M.; Arbabi, A.; Ruan, H.; Faraon, A.; Yang, C. Wavefront Shaping with Disorder-Engineered Metasurfaces. *Nat Photonics* **2018**, *12* (2). https://doi.org/10.1038/s41566-017-0078-z.

(66) Tiwari, P.; Srivastava, A. K.; Khattak, B. Q.; Verma, S.; Upadhyay, A.; Sinha, A. K.; Ganguli, T.; Lodha, G. S.; Deb, S. K. Structural Modification of Poly (Methyl Methacrylate) Due to Electron Irradiation. *Measurement* **2014**, *51* (1), 1–8. https://doi.org/10.1016/j.measurement.2014.01.017.

(67) Kim, J.; Batagoda, T.; Lee, J.; Sylvinson, D.; Ding, K.; Saris, P. J. G.; Kaipa, U.; Oswald, I. W. H.; Omary, M. A.; Thompson, M. E.; Forrest, S. R. Systematic Control of the Orientation of Organic Phosphorescent Pt Complexes in Thin Films for Increased Optical Outcoupling. *Advanced Materials* **2019**, *31* (32), 1900921. https://doi.org/10.1002/adma.201900921.

(68) Sidhik, S.; Li, W.; Samani, M. H. K.; Zhang, H.; Wang, Y.; Hoffman, J.; Fehr, A. K.; Wong, M. S.; Katan, C.; Even, J.; Marciel, A. B.; Kanatzidis, M. G.; Blancon, J. C.; Mohite, A. D. Memory Seeds Enable High Structural Phase Purity in 2D Perovskite Films for High-Efficiency Devices. *Advanced Materials* **2021**, *33* (29). https://doi.org/10.1002/adma.202007176.

(69) Stoumpos, C. C.; Cao, D. H.; Clark, D. J.; Young, J.; Rondinelli, J. M.; Jang, J. I.; Hupp, J. T.; Kanatzidis, M. G. Ruddlesden–Popper Hybrid Lead Iodide Perovskite 2D Homologous Semiconductors. *Chemistry of Materials* **2016**, *28* (8), 2852–2867. https://doi.org/10.1021/acs.chemmater.6b00847.

(70) Blancon, J. C.; Tsai, H.; Nie, W.; Stoumpos, C. C.; Pedesseau, L.; Katan, C.; Kepenekian, M.; Soe, C. M. M.; Appavoo, K.; Sfeir, M. Y.; Tretiak, S.; Ajayan, P. M.; Kanatzidis, M. G.; Even, J.; Crochet, J. J.; Mohite, A. D. Extremely Efficient Internal Exciton Dissociation through Edge States in Layered 2D Perovskites. *Science (1979)* **2017**, *355* (6331). https://doi.org/10.1126/science.aal4211.

(71) Kamau, S.; Hou, J.; Hurley, N.; Alnasser, K.; Sidhik, S.; Hathaway, E.; Gonzalez Rodriguez, R.; Kaul, A.; Cui, J.; Mohite, A.; Lin, Y. Reversible and Irreversible Layer Edge Relaxation in Laser-Radiation-Hardened 2D Organic–Inorganic Perovskite Crystals. *physica status solidi (RRL) – Rapid Research Letters* **2023**. https://doi.org/10.1002/pssr.202300221.

(72) Oskooi; F., A.; et al.; Oskooi, A. F.; Roundy, D.; Ibanescu, M.; Bermel, P.; Joannopoulos, J. D.; Johnson, S. G. MEEP: A Flexible Free-Software Package for Electromagnetic Simulations by the FDTD Method. *Comput Phys Commun* **2010**, *181* (3).

(73) Rakić, A. D.; Djurišić, A. B.; Elazar, J. M.; Majewski, M. L. Optical Properties of Metallic Films for Vertical-Cavity Optoelectronic Devices. *Appl Opt* **1998**, *37* (22), 5271. https://doi.org/10.1364/AO.37.005271.

(74) Wang, M.; Tang, J.; Wang, H.; Zhang, C.; Zhao, Y. S.; Yao, J. Grain Boundary Enhanced Photoluminescence Anisotropy in Two-Dimensional Hybrid Perovskite Films. *Adv Opt Mater* **2020**, *8* (7). https://doi.org/10.1002/adom.201901780.

(75) Tuong Ly, K.; Chen-Cheng, R. W.; Lin, H. W.; Shiau, Y. J.; Liu, S. H.; Chou, P. T.; Tsao, C. S.; Huang, Y. C.; Chi, Y. Near-Infrared Organic Light-Emitting Diodes with Very High External Quantum Efficiency and Radiance. *Nat Photonics* **2017**, *11* (1). https://doi.org/10.1038/nphoton.2016.230.

(76) Kim, K. H.; Kim, J. J. Origin and Control of Orientation of Phosphorescent and TADF Dyes for High-Efficiency OLEDs. *Advanced Materials*. 2018. https://doi.org/10.1002/adma.201705600.

(77) Zhou, L.; Ou, Q. D.; Li, Y. Q.; Xiang, H. Y.; Xu, L. H.; Chen, J. de; Li, C.; Shen, S.; Lee, S. T.; Tang, J. X. Efficiently Releasing the Trapped Energy Flow in White Organic Light-Emitting Diodes with Multifunctional Nanofunnel Arrays. *Adv Funct Mater* **2015**, *25* (18). https://doi.org/10.1002/adfm.201500310.

(78) Song, B.; Hou, J.; Wang, H.; Sidhik, S.; Miao, J.; Gu, H.; Zhang, H.; Liu, S.; Fakhraai, Z.; Even, J.; Blancon, J.-C.; Mohite, A. D.; Jariwala, D. Determination of Dielectric Functions and Exciton Oscillator Strength of Two-Dimensional Hybrid Perovskites. *ACS Mater Lett* **2021**, *3* (1), 148–159. https://doi.org/10.1021/acsmaterialslett.0c00505.

(79) C. Kittel, Introduction to Solid State Physics, 8thed. (John Wiley and Sons, New York, 2004).

(80) Liu, H.; Chen, X. Nonlinear Moiré Superlattice for Super-Resolution Nondestructive Detection of Nonlinear Photonic Crystals. *Laser Photon Rev* **2021**, *15* (10), 20000596. https://doi.org/10.1002/lpor.202000596.

Supporting information for

Fabrications of twisted moiré photonic crystal and random moiré photonic crystal and their potential applications in light extraction

Khadijah Alnasser,[1] Shan Li,[2] Siraj Sidhik,[3] Steve Kamau,[1] Jin Hou,[3] Noah Hurley,[1] Ayman Alzaid,[4] Sicheng Wang,[2] Hao Yan,[2] Jiangdong Deng,[5] Mohammad Omary,[2] Aditya D Mohite,[6,7] Jingbiao Cui,[1] and Yuankun Lin [1,8,*]

[1]*Department of Physics, University of North Texas, Denton, TX, USA*
[2]*Department of Chemistry, University of North Texas, Denton, TX, USA*
[3]*Department of Materials Science and NanoEngineering, Rice University, Houston, TX, USA*
[4]*Department of Computer Science, New Mexico State University, Las Cruces, NM 88003*
[5]*Center for Nanoscale Systems, Harvard University, Cambridge, MA 02138, USA*
[6]*Department of Chemical and Biomolecular Engineering, Rice University, Houston, TX, USA.*
[7]*Applied Physics Program, Smalley-Curl Institute, Rice University, Houston, TX, USA*
[8]*Department of Electrical Engineering, University of North Texas, Denton, TX, USA*
***correspondence:** yuankun.lin@unt.edu*

Computation Code-I

One example of simulation codes for random twisted photonic crystal:

```
(set! *random-state* (seed->random-state (+ (car time) (cdr time)))))

(set! geometry (list (make block (material glass) (size infinity infinity (+ dpml tglass))
(center 0 0 (- (* 0.5 sz) (* 0.5 (+ dpml tglass)))))
        (make block (material perovskite) (size infinity infinity tito)
         (center 0 0 (- (* 0.5 sz) dpml tglass (* 0.5 tito))))
        (make block (material org) (size infinity infinity torg)
         (center 0 0 (- (* 0.5 sz) dpml tglass tito (* 0.5 torg))))
         (make cylinder (material org) (radius 0.314) (height 0.04) (axis 0 0 1)
         (center 0 0 (- (* 0.5 sz) dpml tglass tito torg (* 0.5 rt))))
         (make cylinder (material org) (radius 0.51) (height 0.04) (axis 0 0 1)
         (center 0 (/ sxy -11.3) (- (* 0.5 sz) dpml tglass tito torg (* 0.5 rt))))
         (make cylinder (material org) (radius 0.51) (height 0.04) (axis 0 0 1)
         (center (/ sxy -14.09) 0 (- (* 0.5 sz) dpml tglass tito torg (* 0.5 rt))))
         (make cylinder (material org) (radius 0.323) (height 0.04) (axis 0 0 1)
         (center (/ sxy -10.89) (/ sxy -13.79) (- (* 0.5 sz) dpml tglass tito torg (* 0.5 rt))))
         (make cylinder (material org) (radius 0.48) (height 0.04) (axis 0 0 1)
         (center (/ sxy -6.15) (/ sxy -13.85) (- (* 0.5 sz) dpml tglass tito torg (* 0.5 rt))))
         (make cylinder (material org) (radius 0.343) (height 0.04) (axis 0 0 1)
         (center (/ sxy -4.15) (/ sxy -8.62) (- (* 0.5 sz) dpml tglass tito torg (* 0.5 rt))))
         (make cylinder (material org) (radius 0.46) (height 0.04) (axis 0 0 1)
```

```
(center (/ sxy -3.09) (/ sxy -13.9) (- (* 0.5 sz) dpml tglass tito torg (* 0.5 rt))))
(make cylinder (material org) (radius 0.32) (height 0.04) (axis 0 0 1)
(center (/ sxy -2.3) (/ sxy -14.08) (- (* 0.5 sz) dpml tglass tito torg (* 0.5 rt))))
(make cylinder (material org) (radius 0.335) (height 0.04) (axis 0 0 1)
(center (/ sxy -2) (/ sxy -14) (- (* 0.5 sz) dpml tglass tito torg (* 0.5 rt))))
(make cylinder (material org) (radius 0.283) (height 0.04) (axis 0 0 1)
(center (/ sxy -5.7) 0 (- (* 0.5 sz) dpml tglass tito torg (* 0.5 rt))))
(make cylinder (material org) (radius 0.43) (height 0.04) (axis 0 0 1)
(center (/ sxy -4.09) 0 (- (* 0.5 sz) dpml tglass tito torg (* 0.5 rt))))
 (make cylinder (material org) (radius 0.284) (height 0.04) (axis 0 0 1)
(center (/ sxy -2.89) 0 (- (* 0.5 sz) dpml tglass tito torg (* 0.5 rt))))
 (make cylinder (material org) (radius 0.34) (height 0.04) (axis 0 0 1)
(center (/ sxy -2.46) 0 (- (* 0.5 sz) dpml tglass tito torg (* 0.5 rt))))
 (make cylinder (material org) (radius 0.335) (height 0.04) (axis 0 0 1)
(center (/ sxy -2) 0 (- (* 0.5 sz) dpml tglass tito torg (* 0.5 rt))))
(make cylinder (material org) (radius 0.314) (height 0.04) (axis 0 0 1)
(center 0 (/ sxy -6.1) (- (* 0.5 sz) dpml tglass tito torg (* 0.5 rt))))
(make cylinder (material org) (radius 0.45) (height 0.04) (axis 0 0 1)
(center 0 (/ sxy -3.75) (- (* 0.5 sz) dpml tglass tito torg (* 0.5 rt))))
(make cylinder (material org) (radius 0.3) (height 0.04) (axis 0 0 1)
(center 0 (/ sxy -2.9) (- (* 0.5 sz) dpml tglass tito torg (* 0.5 rt))))
(make cylinder (material org) (radius 0.365) (height 0.04) (axis 0 0 1)
(center 0 (/ sxy -2.3) (- (* 0.5 sz) dpml tglass tito torg (* 0.5 rt))))
(make cylinder (material org) (radius 0.335) (height 0.04) (axis 0 0 1)
(center 0 (/ sxy -2) (- (* 0.5 sz) dpml tglass tito torg (* 0.5 rt))))
(make cylinder (material org) (radius 0.47) (height 0.04) (axis 0 0 1)
(center (/ sxy -13.7) (/ sxy -5.95) (- (* 0.5 sz) dpml tglass tito torg (* 0.5 rt))))
(make cylinder (material org) (radius 0.334) (height 0.04) (axis 0 0 1)
(center (/ sxy -5.89) (/ sxy -6.09) (- (* 0.5 sz) dpml tglass tito torg (* 0.5 rt))))
(make cylinder (material org) (radius 0.43) (height 0.04) (axis 0 0 1)
(center (/ sxy -4.08) (/ sxy -5.5) (- (* 0.5 sz) dpml tglass tito torg (* 0.5 rt))))
(make cylinder (material org) (radius 0.357) (height 0.04) (axis 0 0 1)
(center (/ sxy -2.9) (/ sxy -6.07) (- (* 0.5 sz) dpml tglass tito torg (* 0.5 rt))))
(make cylinder (material org) (radius 0.42) (height 0.04) (axis 0 0 1)
(center (/ sxy -2.3) (/ sxy -6.45) (- (* 0.5 sz) dpml tglass tito torg (* 0.5 rt))))
(make cylinder (material org) (radius 0.335) (height 0.04) (axis 0 0 1)
(center (/ sxy -2) (/ sxy -6) (- (* 0.5 sz) dpml tglass tito torg (* 0.5 rt))))
(make cylinder (material org) (radius 0.36) (height 0.04) (axis 0 0 1)
(center (/ sxy -13.61) (/ sxy -4.09) (- (* 0.5 sz) dpml tglass tito torg (* 0.5 rt))))
(make cylinder (material org) (radius 0.42) (height 0.04) (axis 0 0 1)
(center (/ sxy -13.75) (/ sxy -2.87) (- (* 0.5 sz) dpml tglass tito torg (* 0.5 rt))))
(make cylinder (material org) (radius 0.315) (height 0.04) (axis 0 0 1)
(center (/ sxy -13.55) (/ sxy -2.35) (- (* 0.5 sz) dpml tglass tito torg (* 0.5 rt))))
(make cylinder (material org) (radius 0.315) (height 0.04) (axis 0 0 1)
(center (/ sxy -14) (/ sxy -2) (- (* 0.5 sz) dpml tglass tito torg (* 0.5 rt))))
(make cylinder (material org) (radius 0.42) (height 0.04) (axis 0 0 1)
```

(center (/ sxy -6.07) (/ sxy -3.9) (- (* 0.5 sz) dpml tglass tito torg (* 0.5 rt))))
(make cylinder (material org) (radius 0.347) (height 0.04) (axis 0 0 1)
(center (/ sxy -5.85) (/ sxy -3.07) (- (* 0.5 sz) dpml tglass tito torg (* 0.5 rt))))
(make cylinder (material org) (radius 0.4) (height 0.04) (axis 0 0 1)
(center (/ sxy -6.1) (/ sxy -2.55) (- (* 0.5 sz) dpml tglass tito torg (* 0.5 rt))))
(make cylinder (material org) (radius 0.315) (height 0.04) (axis 0 0 1)
(center (/ sxy -6) (/ sxy -2) (- (* 0.5 sz) dpml tglass tito torg (* 0.5 rt))))
(make cylinder (material org) (radius 0.32) (height 0.04) (axis 0 0 1)
(center (/ sxy -3.95) (/ sxy -3.75) (- (* 0.5 sz) dpml tglass tito torg (* 0.5 rt))))
(make cylinder (material org) (radius 0.46) (height 0.04) (axis 0 0 1)
(center (/ sxy -4.08) (/ sxy -2.85) (- (* 0.5 sz) dpml tglass tito torg (* 0.5 rt))))
(make cylinder (material org) (radius 0.347) (height 0.04) (axis 0 0 1)
(center (/ sxy -3.89) (/ sxy -2.3) (- (* 0.5 sz) dpml tglass tito torg (* 0.5 rt))))
(make cylinder (material org) (radius 0.315) (height 0.04) (axis 0 0 1)
(center (/ sxy -4) (/ sxy -2) (- (* 0.5 sz) dpml tglass tito torg (* 0.5 rt))))
(make cylinder (material org) (radius 0.43) (height 0.04) (axis 0 0 1)
(center (/ sxy -3.08) (/ sxy -3.92) (- (* 0.5 sz) dpml tglass tito torg (* 0.5 rt))))
(make cylinder (material org) (radius 0.36) (height 0.04) (axis 0 0 1)
(center (/ sxy -2.95) (/ sxy -2.82) (- (* 0.5 sz) dpml tglass tito torg (* 0.5 rt))))
(make cylinder (material org) (radius 0.39) (height 0.04) (axis 0 0 1)
(center (/ sxy -3.09) (/ sxy -2.38) (- (* 0.5 sz) dpml tglass tito torg (* 0.5 rt))))
(make cylinder (material org) (radius 0.315) (height 0.04) (axis 0 0 1)
(center (/ sxy -3) (/ sxy -2) (- (* 0.5 sz) dpml tglass tito torg (* 0.5 rt))))
(make cylinder (material org) (radius 0.366) (height 0.04) (axis 0 0 1)
(center (/ sxy -2.35) (/ sxy -4.09) (- (* 0.5 sz) dpml tglass tito torg (* 0.5 rt))))
(make cylinder (material org) (radius 0.37) (height 0.04) (axis 0 0 1)
(center (/ sxy -2.43) (/ sxy -2.97) (- (* 0.5 sz) dpml tglass tito torg (* 0.5 rt))))
(make cylinder (material org) (radius 0.396) (height 0.04) (axis 0 0 1)
(center (/ sxy -2.35) (/ sxy -2.42) (- (* 0.5 sz) dpml tglass tito torg (* 0.5 rt))))
(make cylinder (material org) (radius 0.335) (height 0.04) (axis 0 0 1)
(center (/ sxy -2.4) (/ sxy -2) (- (* 0.5 sz) dpml tglass tito torg (* 0.5 rt))))
(make cylinder (material org) (radius 0.335) (height 0.04) (axis 0 0 1)
(center (/ sxy -2) (/ sxy -4) (- (* 0.5 sz) dpml tglass tito torg (* 0.5 rt))))
(make cylinder (material org) (radius 0.335) (height 0.04) (axis 0 0 1)
(center (/ sxy -2) (/ sxy -3) (- (* 0.5 sz) dpml tglass tito torg (* 0.5 rt))))
(make cylinder (material org) (radius 0.335) (height 0.04) (axis 0 0 1)
(center (/ sxy -2) (/ sxy -2.4) (- (* 0.5 sz) dpml tglass tito torg (* 0.5 rt))))
(make cylinder (material org) (radius 0.335) (height 0.04) (axis 0 0 1)
(center (/ sxy -2) (/ sxy -2) (- (* 0.5 sz) dpml tglass tito torg (* 0.5 rt))))
(make cylinder (material org) (radius 0.335) (height 0.04) (axis 0 0 1)
(center (/ sxy -2) (/ sxy -2) (- (* 0.5 sz) dpml tglass tito torg (* 0.5 rt))))

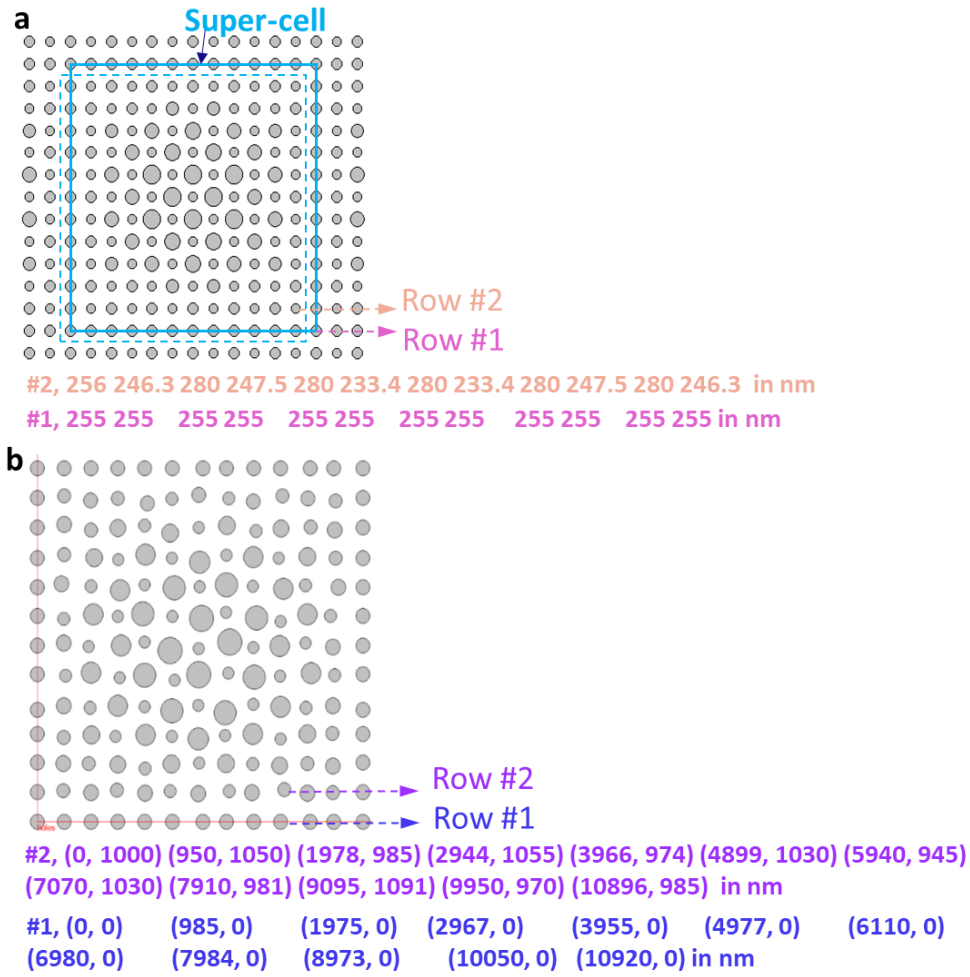

Fig. S1. (a) Unit super-cell as indicated by solid or dashed square for the twisted moiré photonic crystals (PhCs). The diameters of circles in row #1 and #2 inside the dashed square are listed below the super-cell as examples. (b) Unit super-cell for position-randomized moiré PhCs. The positions of circles in row #1 and #2 are listed below the super-cell as examples.

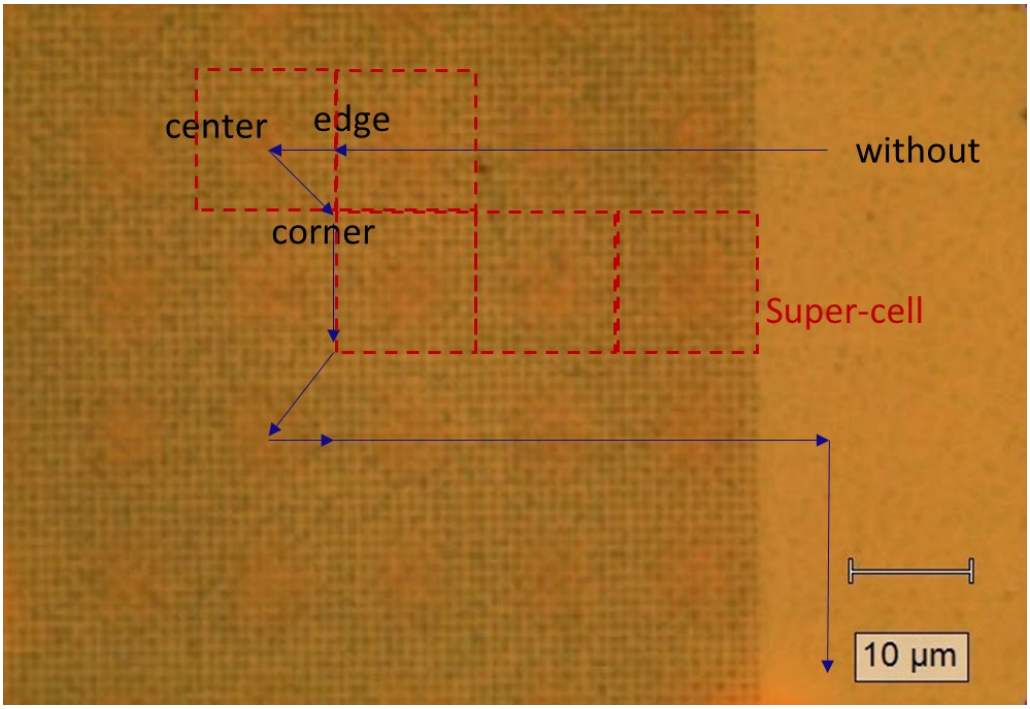

Fig. S2. (a) Optical microscope image of 2D Ruddlesden-Popper perovskites of n=3 on areas with and without moiré PhCs. The super-cell is indicated by the dashed red square. The arrows indicate the photoluminescence measurement orders to make the best effort of same sample thickness for one set of 4 measurements at corner, center and edge of the unit super-cell and at an area without PhCs.

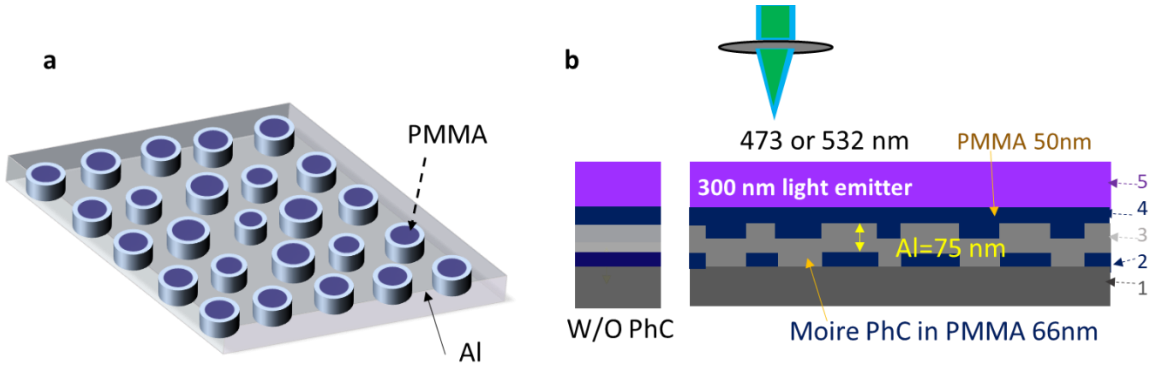

Fig. S3. (a) Schematic of the PMMA cylinders in Al background. (b) Schematic of LED without (left) and with (right) moiré PhCs: PMMA spin-coated on Si substrate (1), e-beam lithography (2), Al deposition (3), PMMA spin-coated on Al (4) and light emitter deposition (5). The light will not pass through the Al layer. We remove the PMMA below the Al layer and Si substrate in the to-be-simulated structure in Fig. S4a.

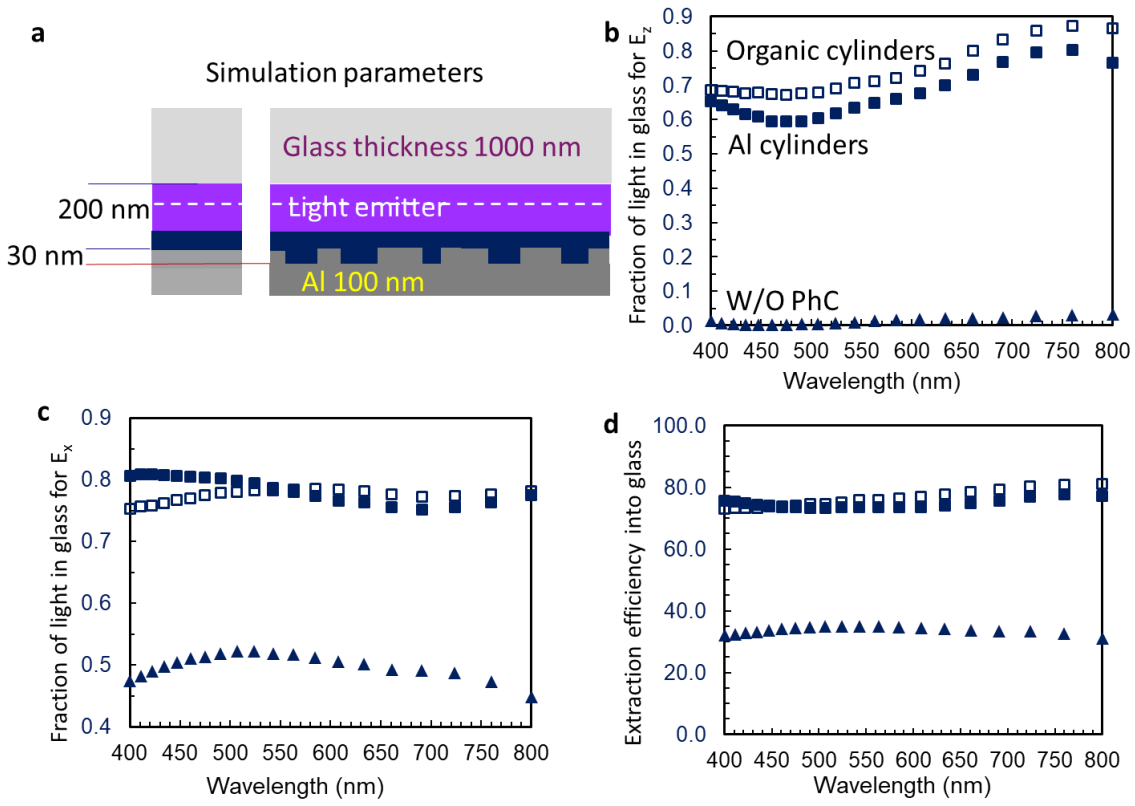

Fig. S4. (a) Schematic of simulated LED without (left) and with (right) moiré PhCs: glass substrate was added for the comparison with traditional LED structure. (b-c) simulated fraction of light in glass for dipole orientations perpendicular to (b) and parallel to (c) the layers of LED with PhCs of organic cylinders in Al background (empty squares), and Al cylinders in organic background (solid squares) and without PhCs (solid triangles). (d) Overall extraction efficiency of light into glass substrate (squares and triangles are for same LED structures as these in (b) and (c)).

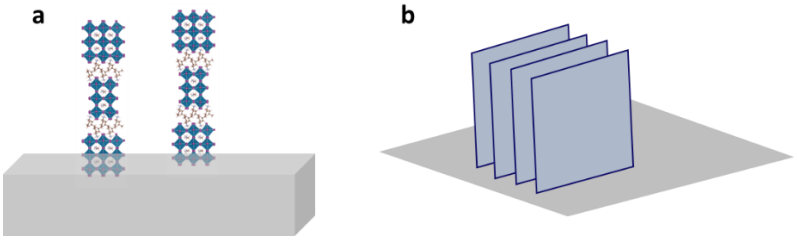

Fig. S5. Schematic of the ordered arrangement of 2D $(BA)_2(MA)_2Pb_3I_{10}$ film (a) and PtD film (b) on the substrate.

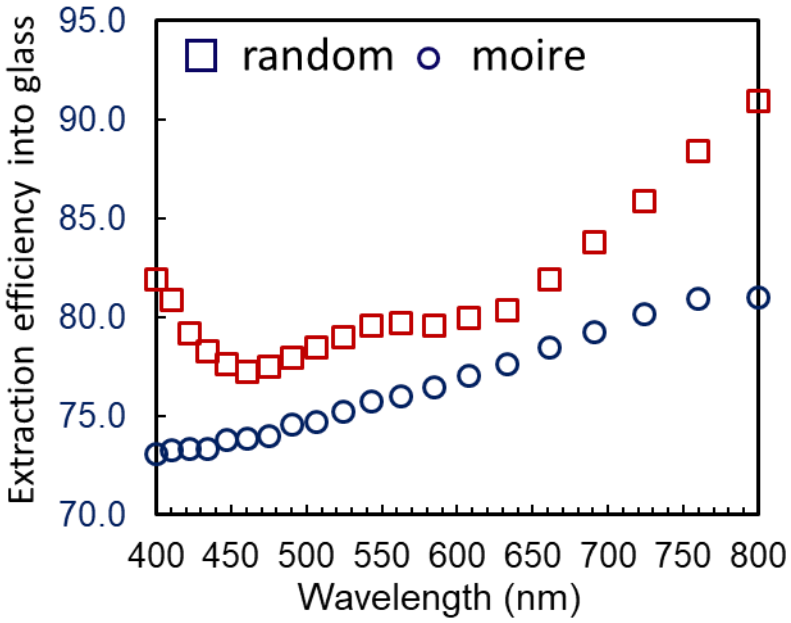

Fig. S6. Overall extraction efficiency of light into glass substrate for LED integrated with random moiré PhC (squares) and with regular moiré PhC (circles) where organic cylinders sit in Al background.